Neurosci. Bull. October, 2022, 38(10):1199–1214
https://doi.org/10.1007/s12264-022-00902-0

www.neurosci.cn
www.springer.com/12264

ORIGINAL ARTICLE

Histones of Neutrophil Extracellular Traps Induce CD11b Expression in Brain Pericytes *Via* Dectin-1 after Traumatic Brain Injury

Yang-Wuyue Liu[1] · Jingyu Zhang[2] · Wanda Bi[1,5] · Mi Zhou[1] · Jiabo Li[1] · Tiantian Xiong[1] · Nan Yang[3] · Li Zhao[4] · Xing Chen[3] · Yuanguo Zhou[3] · Wenhui He[1] · Teng Yang[1] · Hao Wang[2] · Lunshan Xu[2] · Shuang-Shuang Dai[1]

Received: 25 January 2022 / Accepted: 3 May 2022 / Published online: 11 July 2022

Abstract The brain pericyte is a unique and indispensable part of the blood-brain barrier (BBB), and contributes to several pathological processes in traumatic brain injury (TBI). However, the cellular and molecular mechanisms by which pericytes are regulated in the damaged brain are largely unknown. Here, we show that the formation of neutrophil extracellular traps (NETs) induces the appearance of $CD11b^+$ pericytes after TBI. These $CD11b^+$ pericyte subsets are characterized by increased permeability and pro-inflammatory profiles compared to $CD11b^-$ pericytes. Moreover, histones from NETs by Dectin-1 facilitate CD11b induction in brain pericytes in PKC-c-Jun dependent manner, resulting in neuroinflammation and BBB dysfunction after TBI. These data indicate that neutrophil–NET–pericyte and histone–Dectin-1–CD11b are possible mechanisms for the activation and dysfunction of pericytes. Targeting NETs formation and Dectin-1 are promising means of treating TBI.

Keywords Pericyte · Neutrophil · TBI · NET · Dectin-1

Introduction

Overwhelming lymphocyte infiltration and dysfunction of the blood-brain barrier (BBB) are important pathophysiological mechanisms of traumatic brain injury (TBI) [1]. Neutrophils are the most abundant circulating leukocytes that migrate to injury sites and are involved in the initiation and development of the immunological response [2–4]. It has been shown that BBB disruption facilitates the infiltration of neutrophils into brain tissue [5]. However, the cellular and molecular mechanisms by which the BBB loses its "brain guard" functions and interacts with neutrophils after TBI are still less explored.

The BBB is a compact and dense capillary wall that allows few substances to pass into the brain; it is made up of endothelial cells, pericytes, and astrocytes [6]. Pericytes are surrounded by endothelial basement membrane and astrocytic pseudopodia [7]. Of note, pericytes are sensitive and versatile in response to inflammatory stimuli, regulating cerebral blood flow dynamics and leukocyte recruitment under pathological conditions [8, 9]. Proebstl *et al*. found that pericytes are the accomplices of neutrophils under inflammatory conditions, losing their guard function and

Yang-Wuyue Liu, Jingyu Zhang, Wanda Bi, Mi Zhou have contributed equally to this work.

Supplementary Information The online version contains supplementary material available at https://doi.org/10.1007/s12264-022-00902-0.

✉ Hao Wang
wanghaofz@sohu.com

✉ Lunshan Xu
asmczjy@yeah.net

✉ Shuang-Shuang Dai
tmmubiodss66@aliyun.com

[1] Department of Biochemistry and Molecular Biology, School of Basic Medicine, Army Medical University, Chongqing 400038, China

[2] Department of Neurosurgery, Daping Hospital, Army Medical University, Chongqing 400042, China

[3] Molecular Biology Center, State Key Laboratory of Trauma, Burn, and Combined Injury, Daping Hospital, Army Medical University, Chongqing 400042, China

[4] Department of Pathophysiology, College of High Altitude Medicine, Army Medical University, Chongqing 400038, China

[5] Brigade 1 of Medical Undergraduates, School of Basic Medicine, Army Medical University, Battalion 1, Chongqing 400038, China

supporting neutrophil subendothelial migration [10]. Brain pericytes can also be induced to express CD11b, a transmembrane protein found on macrophages and microglia, to form a microglia-like phenotype in models of stroke and Alzheimer's disease [11, 12]. However, if CD11b-expressing ($CD11b^+$) pericytes are formed and function in BBB disruption during TBI is undetermined.

Neutrophil extracellular traps (NETs) are characterized by de-condensed chromatin, perforated membrane, and spilled nucleoplasm in activated neutrophils. NETs are fundamental weapons by which neutrophils catch and kill pathogens, as well as contributors to unintended damage [13, 14]. It has recently been reported that NETs contribute to the initiation and development of several diseases of the central nervous system (CNS) [15–17]. Markers of NET formation, including citrullinated histone H3 (CitH3), neutrophil-derived DNA segments, and peptidylarginine deiminase 4 significantly increase after TBI or stroke [17, 18]. Vaibhav *et al.* reported that NETs are key factors in the exacerbation of TBI severity through aggravating neurovascular injury [18]; Yipp *et al.* demonstrated that NETs generally formed during movement and transmigration and the components of NETs interacted with vascular units/BBB intensively [19]. Therefore, NETs are deeply involved in BBB disruption and may facilitate neutrophil–pericyte interactions.

In this study, we explored the possible relationships between NET formation and the appearance of $CD11b^+$ pericytes in a TBI model. The molecular mechanisms of $CD11b^+$ pericyte formation in damaged brain tissue were further investigated, in order to provide a better understanding of pericyte–neutrophil interactions and BBB dysfunctions in the pathogenesis of TBI.

Materials and Methods

TBI Patients

All studies were approved by the Institutional Research Ethics Committee of Army Medical University, and written informed consent was given by the relatives of each patient in the Department of Neurosurgery, Daping Hospital (Army Special Medical Center). Brain specimens were collected from acute moderate TBI patients (Glasgow coma score of 3–9, within 24 h) while decompressive craniectomy and damaged brain tissue resection were necessary for patient survival (Table S1). All samples were de-identified and coded by the attending surgeon before transport to the laboratory. The specimens were acquired and processed based on Clinical Investigation Ethical Approval from the Army Medical Center (2021004, person in charge: Zhang Jingyu), and stored according to the Principles of Human Sample Preservation in China.

TBI Mouse Model

All animal procedures were approved by The Institutional Animal Care and Use Committee at Army Medical University. Adult mixed-sex C57/BL6 mice (aged 6–8 weeks) were provided by the Animal Center of the Army Medical University and subjected to sham or controlled cortical impact as in our previous report [20]. Briefly, mice were anesthetized using pentobarbital sodium (30 mg/kg) and a craniotomy was made in the middle of the left parietal bone (anterior-posterior 2 mm, medial-lateral 2 mm from bregma). The exposed cortex was impacted by an automatic impact machine (LinTech, Monrovia, CA, USA) using a downstroke (velocity, 2.5 m/s; deformation depth, 3 mm; duration, 150 ms) to create a mouse model of moderate TBI. Sham-operated mice underwent the same anesthetic and surgical procedures without impact. The skin incision was closed by sterile sutures and mice were returned to a clean, warm cage to recover. For drug treatment studies, Laminarin (TLRL-LAM, InvivoGen) and Cl-amidine (S8141, Selleck Chem) dissolved in saline were administered every three days *via* intraperitoneal injection.

Neutrophil Isolation and Treatment

Murine neutrophils were isolated from bone marrow as in our previous report [21]. The purity of harvested cells was > 98%, which was confirmed by fluorescence activated cell sorting (FACS) with a specific marker ($CD11b^+LY6G^+$). Isolated neutrophils were washed three times with cold phosphate-buffered saline (PBS) and re-suspended in Dulbecco's modified Eagle medium (DMEM), containing high glucose and antibiotics without fetal bovine serum (FBS). Neutrophils were treated with/without phorbol 12-myristate 13-acetate (PMA 100 ng/mL; P1585, Sigma-Aldrich) for 30 min. Then, stimulated neutrophils were washed 3 times with DMEM and cultured with fresh DMEM (free of antibiotics and FBS) for another 6 h. The supernatant was harvested by low-speed centrifugation (1,500 rpm, 5 min, 4°C) and purified by high-speed centrifugation (14,000 rpm, 20 min, 4°C) to remove cell debris. The ratio of NET-forming medium to fresh DMEM was 1:3 according to preliminary tests (Fig. S1A, B). Under these conditions, the medium induced CD11b expression without cytotoxicity.

Culture of Murine Brain Pericyte Cell Line (MBVP)

The cell line of mouse brain vascular pericytes (MBVPs) was from ScienCell Research Laboratories (M1200, San Diego). MBVP cells were cultured with DMEM at sub-confluent density according to the supplier's protocol. The peptides Histone 1 (H1917), Histone 3 (12–357), and Histone 4 (12–347) were from Sigma-Aldrich and dissolved in ddH_2O for the subsequent treatments.

Brain Tissue Preparation and Analytic Fluorescence-activated Cell Sorting (FACS)

Mice was sacrificed with CO_2 and perfused transcardially with saline prior to brain dissection. Brain pericytes were sorted was FACS as in a previous study [22]. In brief, brain tissue was digested with research grade Liberase™ TL (05401020001, Sigma Aldrich) and 2 µg/mL DNase I (104159, Roche) for 30 min at 37°C. Cell suspensions were then homogenized and filtered through a 200 mesh sieve to remove undigested tissue blocks. Myelin and debris were removed by 22% Percoll (P4937, Sigma-Aldrich) centrifugation at 560×g at 4°C for 10 min. Pellets with single vascular cells were carefully collected and re-suspended in PBS containing 2% FBS. Single-cell suspensions from brain tissue and cell lines were stained for 30 min at 4°C with specific antibodies (Table S2). Flow cytometry data were analyzed with FlowJo software version 11.

Pericyte Sorting from Brain

After constructing the TBI model, single-cell suspension and antibody incubation from brain tissue were achieved using FACS. Infiltrated immune cells ($CD45^+$) were excluded before pericyte sorting. $CD11b^+$ and $CD11b^-$ pericyte populations were each collected. These sorted cells were washed three times with PBS (containing antibiotic) and cultured with complete DMEM in 24-well plates.

Transwell Experiment

Sorted pericytes were seeded in 24-well plates and cultured for 24 h. Transwell inserts (polyester membranes, 8 µm pore size, ø = 6.5 mm; Corning, NY, USA) were put into plates with freshly-isolated neutrophils (10^6) added to the upper side. After co-culturing for 12 h, migrated neutrophils on the lower side of the Transwell insert were harvested and visualized by Giemsa staining (48900, Sigma-Aldrich). The stained cells were counted using ImageJ.

Western Blotting

Whole-cell lysates were collected and prepared as in our previous report [21], and the western blot procedure was carried out by standard methods. Information on the antibodies for specific proteins are listed in Table S2. Target bands were quantified using ImageJ.

LC-MS Analysis of Cell Metabolites

A liquid-liquid extraction and liquid chromatography-electrospray ionization tandem mass spectrometry (LC-MS) method was applied to determine the metabolites in cell culture media. Primary isolated murine neutrophils were treated with or without PMA (100 ng/mL) for 30 min, then incubated with DMEM (free of antibiotics and FBS) for 6 h. Subsequently, culture medium was collected by high speed centrifugation and lyophilized for the following steps [23]. Each group contained 7 individual samples and differential molecules with $P < 0.05$ (statistically different between groups) were screened out.

TMT Proteomics Analysis of Cell Culture Medium

The Tandem Mass Tags (TMT) labeled quantitative proteomics method was applied to analyze total protein in neutrophil-culture medium. Proteins with changes > 1.5-fold and $P < 0.05$ were considered differentially-expressed, and bioinformatics analysis was applied as previously reported [24].

Immunohistochemistry

After anesthesia, mice were perfused transcardially with 0.9% NaCl, then the brain was immediately frozen and embedded in OCT (4583, Tissue-Tek). Brain sections (10 µm) were incubated with primary antibodies (Table S2) diluted in 5% bovine serum albumin (V900933, Sigma-Aldrich) containing 0.1% Triton X-100 (T8787, Sigma-Aldrich). Finally, the sections were stained with DAPI and secondary antibodies and photographed under a fluorescence microscope (Olympus IX-81).

Quantitative Real-time PCR (qRT-PCR)

Total RNA was extracted from cells using the TRIzol reagent protocol (15596018, Thermo Fisher). RNA samples were reverse-transcribed to cDNA using a Reverse Kit (DRR047S, Takara). qRT-PCR was performed on a Bio-Rad iCycler (Version 3.0A). The ΔΔCt method was used to calculate relative mRNA levels in treatment groups

compared to controls. The primer sequences are listed in Table S3.

Trans-epithelial Electrical Resistance (TEER) Measurement

Transwell inserts (polyester membranes, 3 μm pore size, ø = 6.5mm; Corning, NY, USA) were coated with pericyte cell line MBVPs in 24-well plates (10^5/cm^2). The Millicell-ERS (Electrical Resistance System, MERS00002, Millipore) was inserted between the upper chamber and the lower well while measurements took place. TEER values were obtained from continuous impedance measurements as described previously [25]. Once the TEER value of each insert reached > 200 Ω/cm^2 (typically after 2–3 days), cells were treated with NET-induced medium as described above or combined with other treatments (as shown in figures), and TEER measurements were recorded every 2 h. TEER data were recorded as Ω/cm^2 and are presented as percentage (%) relative to the initial value in the control group.

Evans Blue Assay

Evans Blue solution (2%, 4 mL/kg, E8010, Solarbio) was injected intravenously after TBI. The stain was allowed to circulate for 30 min, 6 h, or 24 h. Afterwards, the mice were sacrificed and transcardially perfused with 50 mL ice-cold PBS. The injured left hemisphere was removed and weighed. Then the brain tissue was homogenized in 1 mL PBS, centrifuged for 30 min (14,000 rpm at 4°C). An equal amount of 50% trichloroacetic acid was added to each 500 μL of supernatant and incubated overnight at 4°C. The supernatant was then centrifuged (30 min, 14,000 rpm at 4°C) and measured with an Infinite M200 plate reader (excitation at 620 nm; emission at 680 nm). PBS with 50% trichloroacetic acid was regarded as blank, and gradient doses of Evans Blue were measured to construct a standard curve. The results were quantified according to the standard curve and are presented as (μg of Evans Blue stain)/(g of brain tissue).

Plasmid Construction

The 5′-UTR sequence of the mouse *CD11b* gene was obtained from Pubmed (http://www.ncbi.nlm.nih.gov/entrez/) and then analyzed for potential c-Jun (AP-1) binding sites using web-based algorithms (NUBIScan and hTFtarget) as in our previous report [26]. A fragment containing the mouse *CD11b* gene promoter region (−2900 to +190) was chemically synthesized by Sangon (Shanghai, China) and cloned into the pGL3-basic vector. All the resulting plasmids were named pGFs (see Fig. 8A).

Dual-Luciferase Reporter Assay

MBVPs were transiently transfected with reporter plasmids (pGFs) using Lipofectamine 3000 (L3000008, Thermo Fisher). Two hours later the culture medium was replaced with fresh complete DMEM. After 24 h incubation, specific drugs were added to NET-formed or normal medium and incubated for another 24 h. Then the cell lysates were collected and luciferase activity was measured with a dual-luciferase reporter system according to the manufacturer's instructions (E1910, Promega). The transfection experiments were repeated three times in triplicate, and the transfection efficiency was normalized by dividing firefly luciferase activity by *Renilla* luciferase activity.

Chromatin Immunoprecipitation (ChIP) Assays

ChIP assays were applied using the Pierce™ ChIP assay kit (26157, Thermo Fisher) according to the manufacturer's instructions. The targeted protein-DNA mixture was gathered by PureProteome Magnet (LSKMAGS08, Millipore). Then the final DNA extracts were analyzed by RT-PCR with specific primers (Table S4). The antibodies against c-Jun and the control IgG were from CST and Beyotime, respectively (listed in Table S2).

Neurobehavioral Evaluations

Open-Field Test

Mice were tested in a square box (40 cm × 40 cm × 40 cm) for 10 min, and activity was digitally recorded as in our previous report [27]. Travel distance, mean velocity, and time spent in the center zone were analyzed with Ethovision XT video-tracking software (Noldus Information Technology, Asheville, NC).

Foot-Fault Test

The experiments were carried out on an elevated beam (2.5 cm × 75 cm) raised 76 cm above the floor as previously described [28]. Mice were placed at the beginning of the beam and their movements were monitored from the beginning to the end. An individual foot fault was identified when a paw slipped completely off the beam while walking. The average foot fault score was calculated from the total steps within 75 cm in three separate trials.

Statistical Analysis

All data were analyzed and presented by using GraphPad Prism version 5.01 (GraphPad Software). Unpaired two-tailed Student *t* test was applied to compare treated groups

with vehicle controls. To analyze parameters depending on two or more factors, two-way ANOVA/multivariate analysis of variance were used with Bonferroni correction. $P < 0.05$ was considered statistically significant. Data in figures are all represented as the mean ± SEM with $*P < 0.05$, $**P < 0.01$, $***P < 0.001$. The number of animals and experimental repeats are noted in the figure legends.

Results

CD11b$^+$ Pericytes Detected in the Brains of TBI Patients and Mice are Characterized by Pro-inflammatory Profiles

Previous studies have shown that CD11b$^+$ pericytes are associated with enhanced phagocytosis and BBB disruption in models of AD or stroke [11, 12]. However, the presence of CD11b$^+$ pericytes in TBI model was still undetermined. Using triple-labeling immunofluorescence, we confirmed the presence of CD11b$^+$ pericytes (marked with PDGFRβ or α-SMA) in brain tissue from TBI patients (Fig. 1A, B) and mice (Fig. 1C, D. Next, we used FACS to specifically distinguish brain pericytes (CD45$^-$CD31$^-$CD13$^+$) from brain tissue based on a previous study [22] (Fig. 2A) and the results showed that CD11b$^+$ pericytes were significantly increased in damaged brain 24 h after TBI compared to Sham (Fig. 2B, C, S1C). In order to explore the differences between CD11b$^+$ and CD11b$^-$ pericytes, we sorted these subpopulations from the damaged brains of TBI mice and prepared them for RNA-seq and Transwell experiments. As shown in Fig. 2D, CD11b$^+$ pericytes were more effective in attracting neutrophils to migrate across the membrane than CD11b$^-$ pericytes. RNA-seq further showed that the mRNA levels of pro-inflammatory genes (*TNF-α, IL-1β, CCL2/5,* and *CXCL8/10*) and BBB disruption-related molecules (*MMP2 and MMP9*) in CD11b$^+$ pericytes were significantly higher than in CD11b$^-$ pericytes (Fig. 2E, F, S2). Meanwhile, we re-checked the RNA-seq data and found that these sorted pericytes expressed relatively low mRNA levels of CD163 (macrophage marker gene) and TMEM119 (microglia marker gene), indicating that these cells were neither BBB-associated macrophages nor microglia (Fig. 2F). The increased mRNA levels of pro-inflammatory molecules (*TNF-α, IL-1β, CCL5,* and *MMP9*) in CD11b$^+$ pericytes were also verified by RT-PCR (Fig. 2G). These data provided evidence that the percentage of CD11b$^+$ pericytes in the brain after TBI was markedly increased and characterized by a pro-inflammatory profile. These CD11b$^+$ pericytes are possibly important contributors to neuroinflammation and BBB disruption in the pathogenesis of TBI.

NET Formation is Enhanced in TBI and NET-formed Medium Induces Significant CD11b Expression in Pericytes

It has been demonstrated that NET formation is strongly increased under inflammatory conditions [17, 18]. Our data reiterated the conclusion that neutrophils in blood from TBI mice more easily form NET structure with PMA stimulation (Fig. 3A). FACS experiments further showed that the percentage of NET formation (CD11b$^+$LY6G$^+$MPO$^+$CitH3$^+$) from the brain parenchyma of TBI mice was relatively high (Fig. 3B–D), consistent with Vaibhav's work [18]. Meanwhile, the neutrophil infiltration rate was positively associated with the proportion of CD11b$^+$ pericytes in damaged brain tissue (Fig. 3E). Thus, we speculated that NET formation is related to CD11b induction on pericytes. To test this hypothesis, we treated a pericyte cell line (MVBPs) with NET-formed medium under established conditions (clear effects without strong cytotoxicity; Fig. S1). After culture with NET-induced medium (with PMA) for 48 h, FACS analysis showed that CD11b expression was strongly induced in MVBPs (Fig. 4A, B). Immunofluorescence, western blotting (WB), and RT-PCR experiments also supported the conclusion that NET-formed medium increased CD11b expression and decreased the level of the tight-junction protein ZO-1 *in vitro* (Fig. 4C–E). TEER experiments further showed that NET-formed medium dramatically jeopardized pericyte integrity (Fig. 4F). All the effects mediated by NET-induced medium were inhibited by Cl-Amidine (a NET formation inhibitor by decreasing peptidylarginine deaminase activity), suggesting that NET formation is associated with CD11b induction in pericytes.

Histones are the Main Components by which NETs Drive CD11b Induction in Pericytes

We next aimed to investigate what components of NET-formed medium drove CD11b induction in pericytes. We collected the cultured medium after removing neutrophils with or without PMA stimulation for proteomics and metabolomics analysis (Fig. 5A). In proteomics analysis, 4,098 proteins were identified in these two groups. Proteins with repeatable fold changes > 1.2 or < 0.8 were screened out as differentially-expressed molecules (Figs 5B, S2). In PMA-stimulated groups, 101 up-regulated and 3 down-regulated proteins were identified. Of note, histones accounted for 30% of the top up-regulated proteins and other neutrophil intracellular molecules (such as lactoferrin, complement 3, and metalloproteinase) were also detectable, consistent with reported the characteristics of NETs [14]. NET formation induced by PMA also caused dramatic alterations in amino-acids, such as N-acetyl-L-cysteine, L-isoleucine, and L-glutamate (Figs 5C, S3). In order to test their effects on

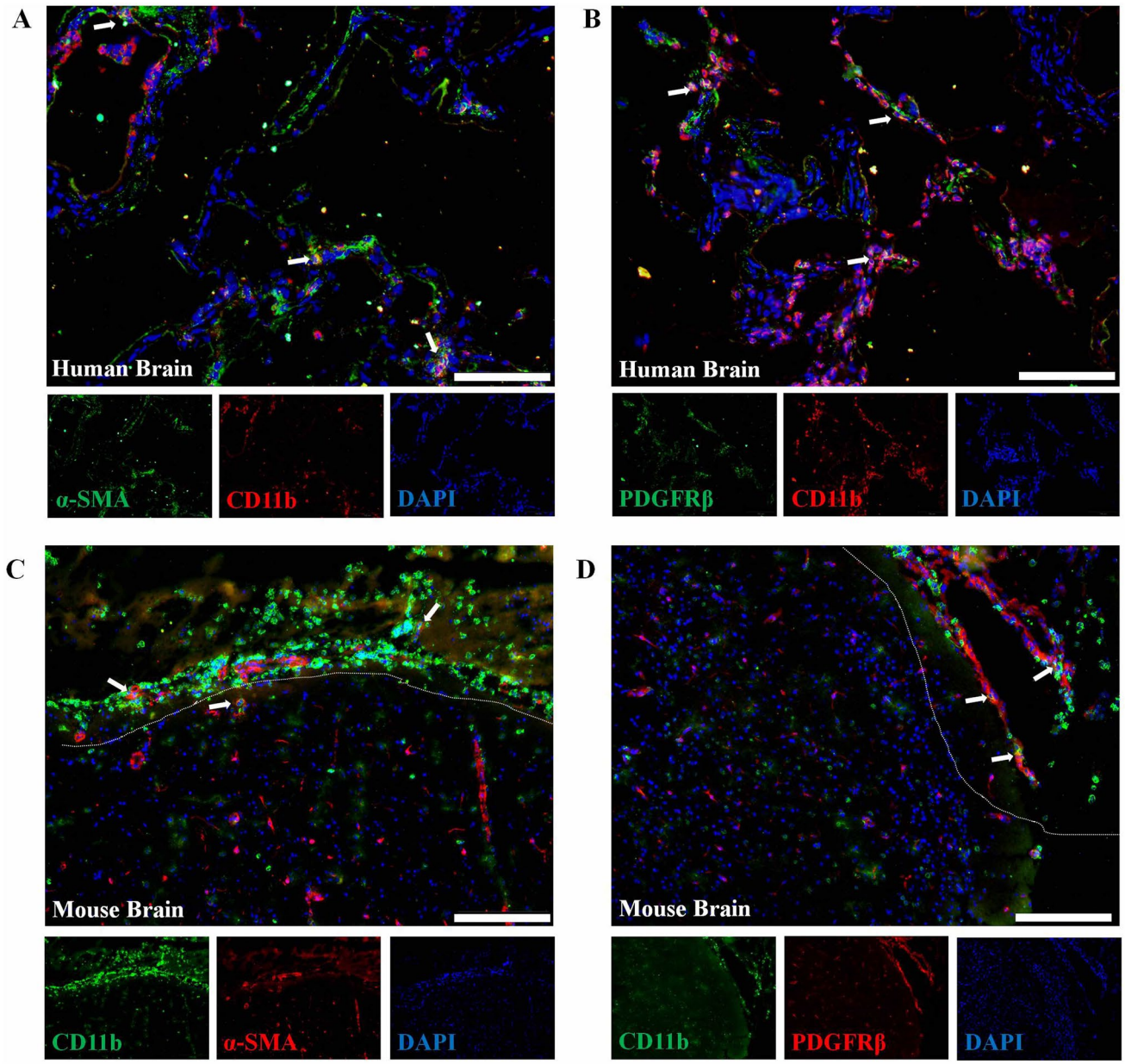

Fig. 1 Immunofluorescence of PDGFRβ and CD11b in damaged brain tissue. **A, B** Immunostaining of the pericyte marker PDGFRβ/α-SMA (green) and CD11b (red) in brain tissue from a TBI patient. **C, D** Immunostaining of the pericyte marker PDGFRβ/α-SMA (red) and CD11b (green) in brain tissue from a TBI mouse. Damaged tissue is marked by dotted lines. Human and mouse brain tissues were collected within 24–48 h after TBI. Scale bars, 100 μm. Cell nucleus are stained with DAPI (blue).

pericytes, we selected some of these proteins (histones and lactoferrin) or metabolites (N-acetyl-L-cysteine and L-isoleucine) to determine whether they change CD11b expression *in vitro*. As shown in Fig. 5D, histones increased the CD11b mRNA levels 24 h after treatment. WB and FACS analysis also showed that histone treatment mediated CD11b induction and ZO-1 downregulation on pericytes in a dose-dependent manner (Fig. 5E, F). We did not find alterations in CD11b mRNA levels (Fig. S4) with specific concentrations of lactoferrin, N-acetyl-L-cysteine, and L-isoleucine based on previous studies [29, 30], indicating that these metabolites/amino-acids are not factors that drive CD11b induction in pericytes.

Dectin-1 is Fundamental for Pericytes to Respond to Histones of NETs *in vitro*

After defining histones as the main components of NETs to affect pericytes, we aimed to decipher the possible ways that pericytes might respond. According to previous

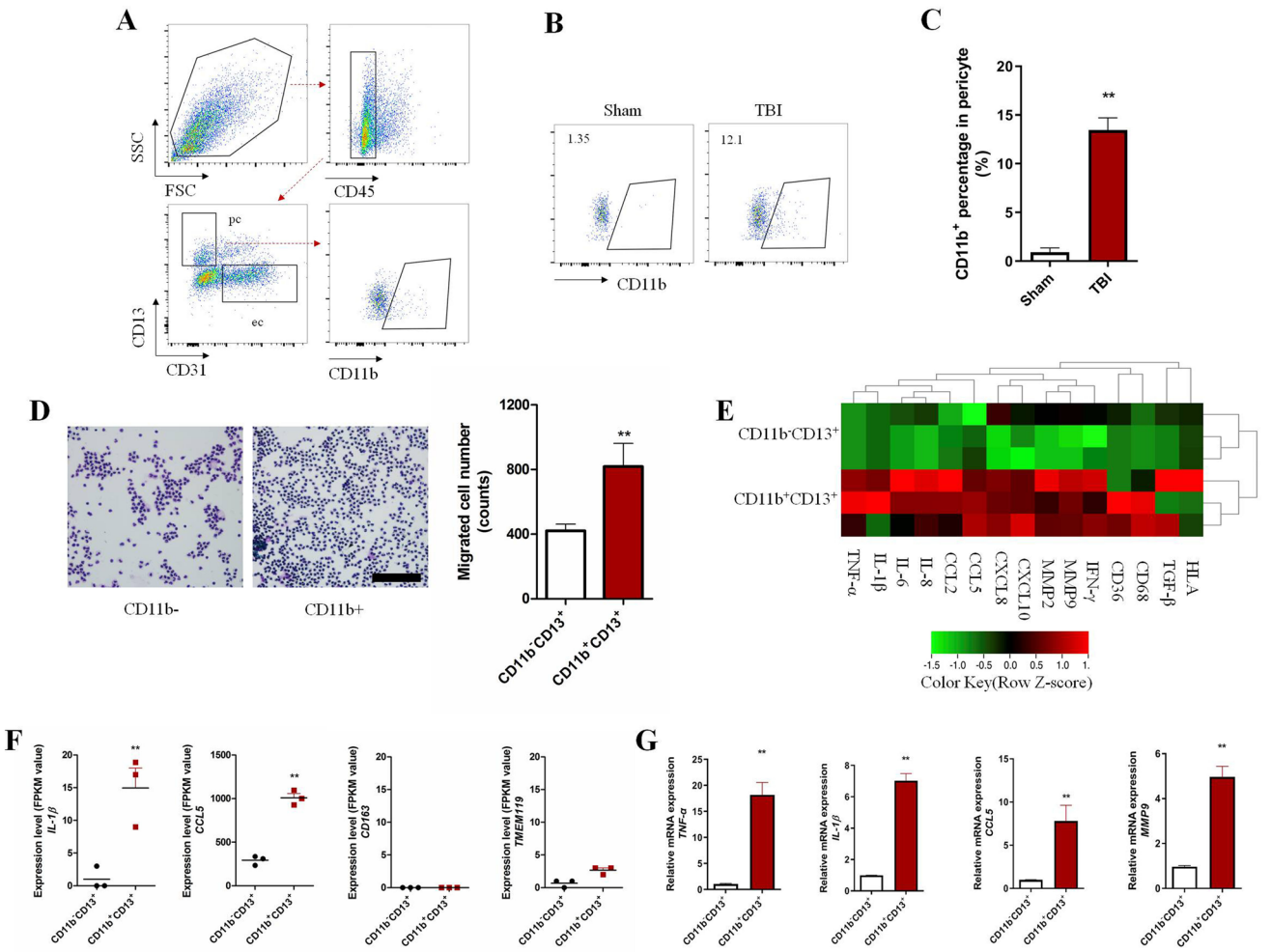

Fig. 2 Functional and molecular features of CD11b-positive pericytes. **A** Flow cytometric diagram of $CD11b^+$ pericytes in brain tissue. **B** Plots of $CD11b^+$ pericytes from Sham and TBI mice. **C** Quantification of $CD11b^+$ pericytes in brain tissue from Sham and TBI mice (n = 5 per group). **D** Neutrophil migration mediated by $CD11b^+$ and $CD11b^-$ pericytes (scale bar, 100 μm). **E** RNA-sequencing data of sorted cells ($CD11b^+CD13^+$ and $CD11b^-CD13^+$) from damaged brain tissue (red, high expression; green, low expression; black, unchanged expression). **F** Expression levels (FPKM value) of cytokine (*IL-1β*), chemokine (*CCL5*), macrophage marker (*CD163*), and microglial marker (*TMEM119*) in sorted cells. **G** Relative mRNA levels of target genes in the $CD11b^+$ population compared to $CD11b^-$ pericytes. Data are shown as the mean ± SEM of 3–5 individual experiments; $^{**}P < 0.01$, two-tailed unpaired Student's t test.

studies, we switched our attention to C-type lectin receptors (CLRs), a large family of transmembrane receptors that recognize not only fungal moieties, but also histone-related molecules from dead cells [31, 32]. Three types of CLR are classified based on their molecular structures: type I, type II and soluble type. Of these, Type II CLRs are the main receptors for the recognition of histone sequences or histone deacetylase complexes released from disintegrated DNA [31, 33]. Type II CLRs carry a conserved carbohydrate-recognition domain and contain five receptors: Dectin-1, Dectin-2, macrophage-inducible CLR (Mincle), dendritic cell-specific ICAM3-grabbing nonintegrin (DC-SIGN), and DC-NK lectin group receptor-1 (DNGR-1) [34]. Based on the human protein atlas database (https://www.proteinatlas.org/), the expression of type II CLRs in the CNS was relatively low except for Dectin-1 and DNGR-1 (Fig. S5A). The protein expression and glycosylation level of Dectin-1 was markedly upregulated in MVBPs with PMA-induced medium or histones (Fig. 6A). This demonstrated that Dectin-1 expression was positively associated with CD11b upregulation in brain pericytes. In order to confirm that Dectin-1 was responsible for CD11b upregulation, Dectin-1 siRNAs and the specific antagonist Laminarin (LAM) were introduced in the subsequent experiments. WB showed that synthetic siRNAs were capable of interfering with Dectin-1 protein expression in the presence of NET-medium and histones (Fig. 6B). Antagonizing Dectin-1 with LAM as well as

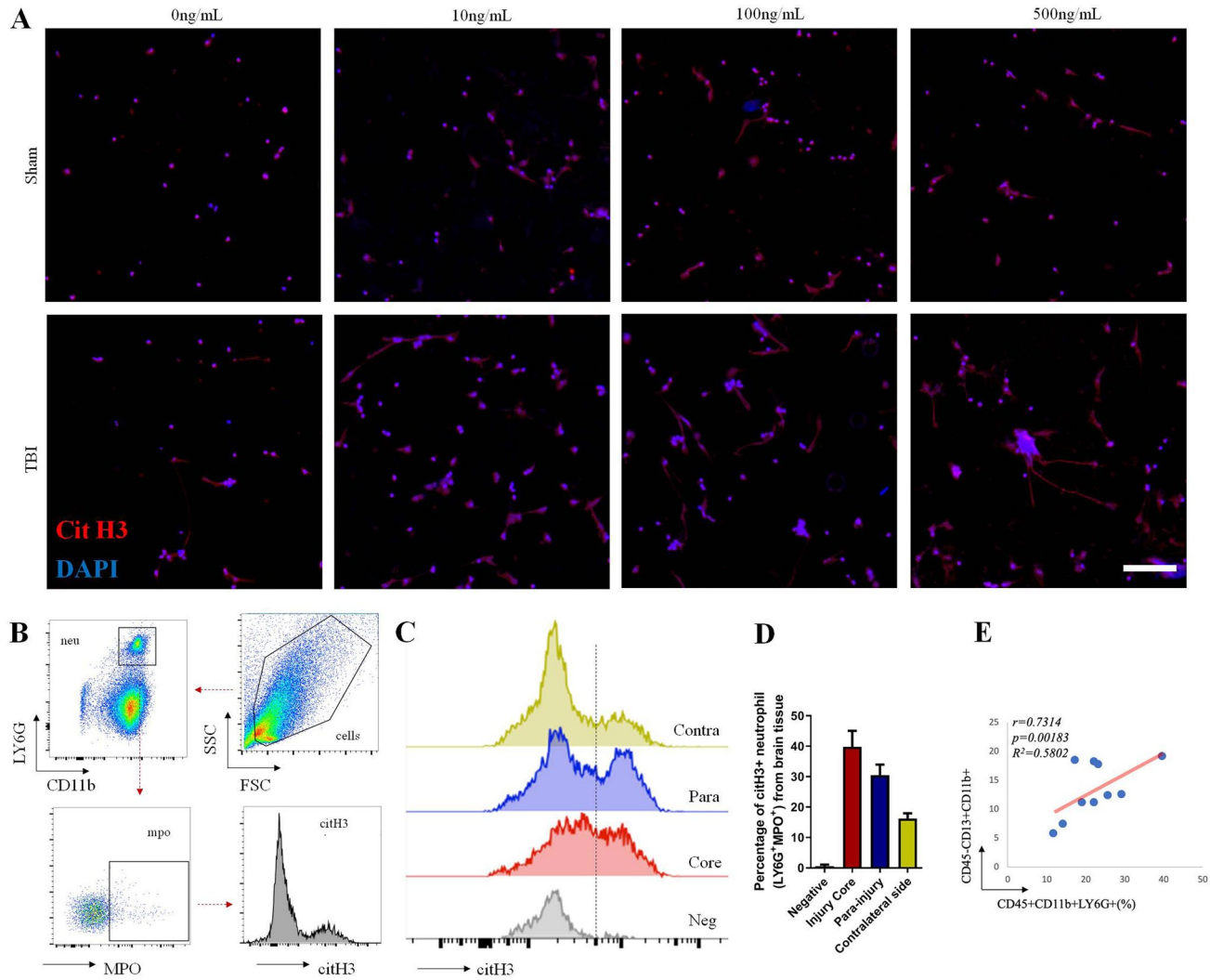

Fig. 3 NET formation after TBI. **A** Immunofluorescence of NET formation in peripheral blood. The neutrophils were isolated from peripheral blood of Sham and TBI mice at 24 h post-injury. Then they were treated with gradient concentrations of PMA (10, 100, and 500 ng/mL) for 6 h and stained with Cit H3 (red) and DAPI (blue) (scale bar 100 μm). **B** Flow cytometric diagram of NET formation ($CitH3^+LY6G^+MPO^+$) in brain tissue. **C** Cit H3 levels in MPO^+ neutrophils from different brain tissues post-TBI. Negative for $LY6G^+MPO^+$ neutrophils without Cit H3 antibody staining. Brain tissues were collected from the injury core, the para-injury area, and the contralateral side of TBI mice. **D** Quantification of Cit H3-positive neutrophils in **C**. Each bar represents 3 individual experiments. Data are shown as the mean ± SEM. **E** Correlation analysis between percentage of neutrophils and CD11b+ pericyte frequency in damaged brain (n = 10).

blocking Dectin-1 expression with siRNAs decreased the CD11b mRNA levels compared to PMA-medium alone (Fig. 6C, D). This phenomenon was consistent with the histone-treated groups (Fig. 6E, F). TEER experiments also confirmed that blocking Dectin-1 (LAM or siRNAs) was beneficial for restoring pericyte integrity *in vitro* (Fig. 6G, H). These results showed that the Dectin-1 antagonist LAM and siRNAs were competent to blunt the CD11b expression mediated by NET medium or histone stimulation, confirming that Dectin-1 was indispensable for pericytes to react to the histones of NETs.

PKCζ/λ and c-Jun Activation Mediated by Dectin-1 are Responsible for CD11b Induction of Pericytes during NET and Histone Treatments

Next, we explored the possible signaling pathways mediated by Dectin-1 that were involved in CD11b induction. From the literature, we discerned that protein kinase Cζ/λ (PKCζ/λ) and the transcriptional factor c-Jun were possible molecules downstream of Dectin-1 activation [34]. The levels of phosphorylated PKC (p-PKCζ/λ) and phosphorylated c-Jun (p-c-Jun), the activated forms of these molecules, were significantly increased following treatment

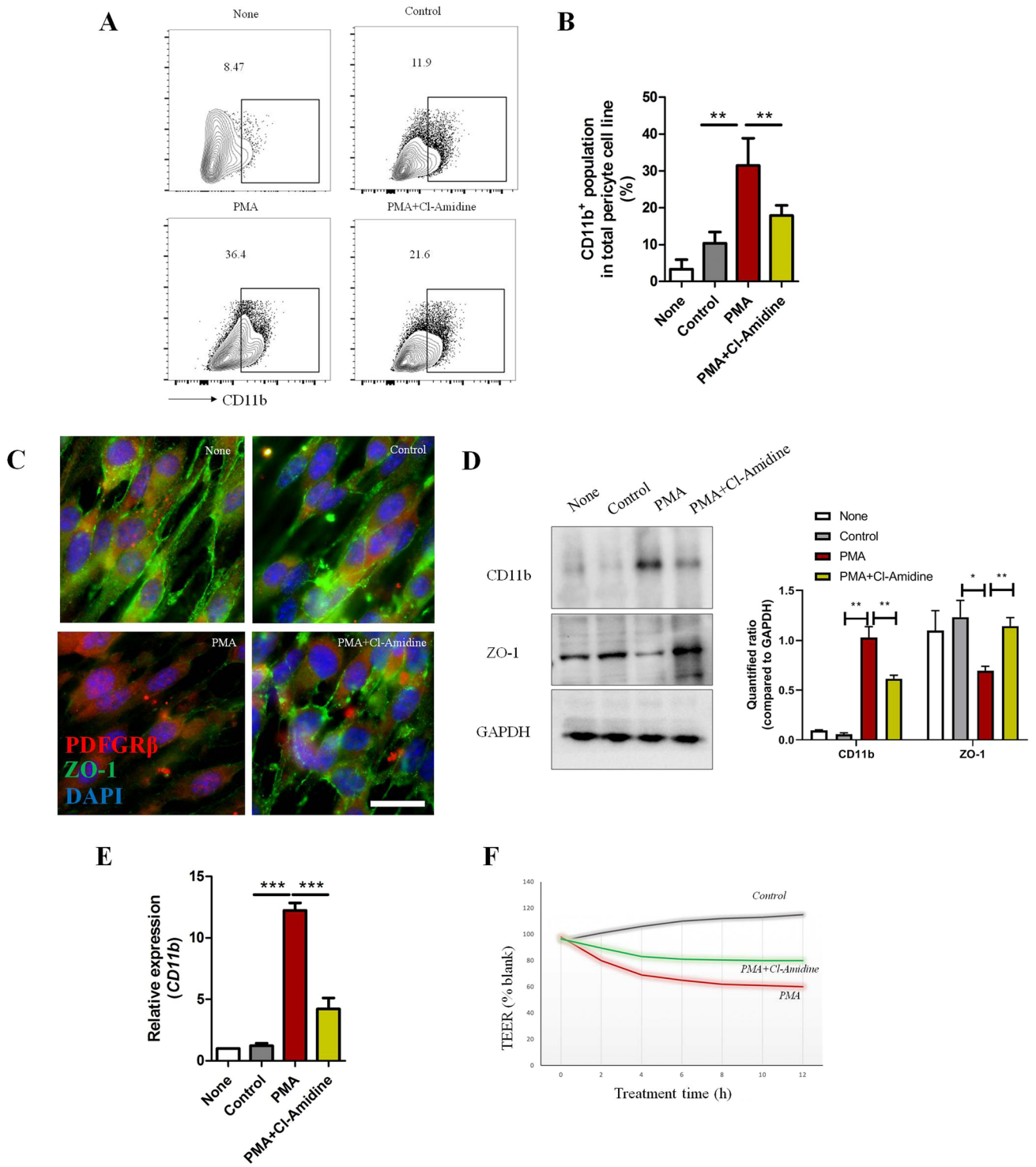

Fig. 4 Effects of NET-formed medium on pericytes. MBVPs were incubated with specific media for 48 h [none, normal medium; control, medium from non-stimulated neutrophils; PMA, NET-formed medium stimulated by PMA (100 ng/mL); PMA+Cl-Amidine, medium from PMA stimulation (100 ng/mL) combined with NET inhibitor Cl-Amidine (10 μmol/L)]. Supernatant was collected by centrifugation for removing neutrophils. **A** Cytometric analysis of $CD11b^+$ MBVPs after different treatments. **B** Percentage of $CD11b^+$ MBVPs in **A** (n = 3). **C** Immunostaining of tight junction protein (ZO-1, green) and pericyte marker (PDGFRβ, red) on MBVPs (scale bar, 20 μm). **D** WB of CD11b and ZO-1 expression in MBVPs after different treatments (protein levels relative to GAPDH loading control). **E** RT-PCR analysis of relative mRNA levels of CD11b in different treatment groups compared to the none group (5 individual experiments per group). **F** Representative graph of continuous TEER values of MBVPs incubated with different culture media. TEER values of each group were compared to blank (MBVPs with normal culture medium). Data are shown as the mean ± SEM; $^*P < 0.05$, $^{**}P < 0.01$, $^{***}P < 0.001$, ANOVA.

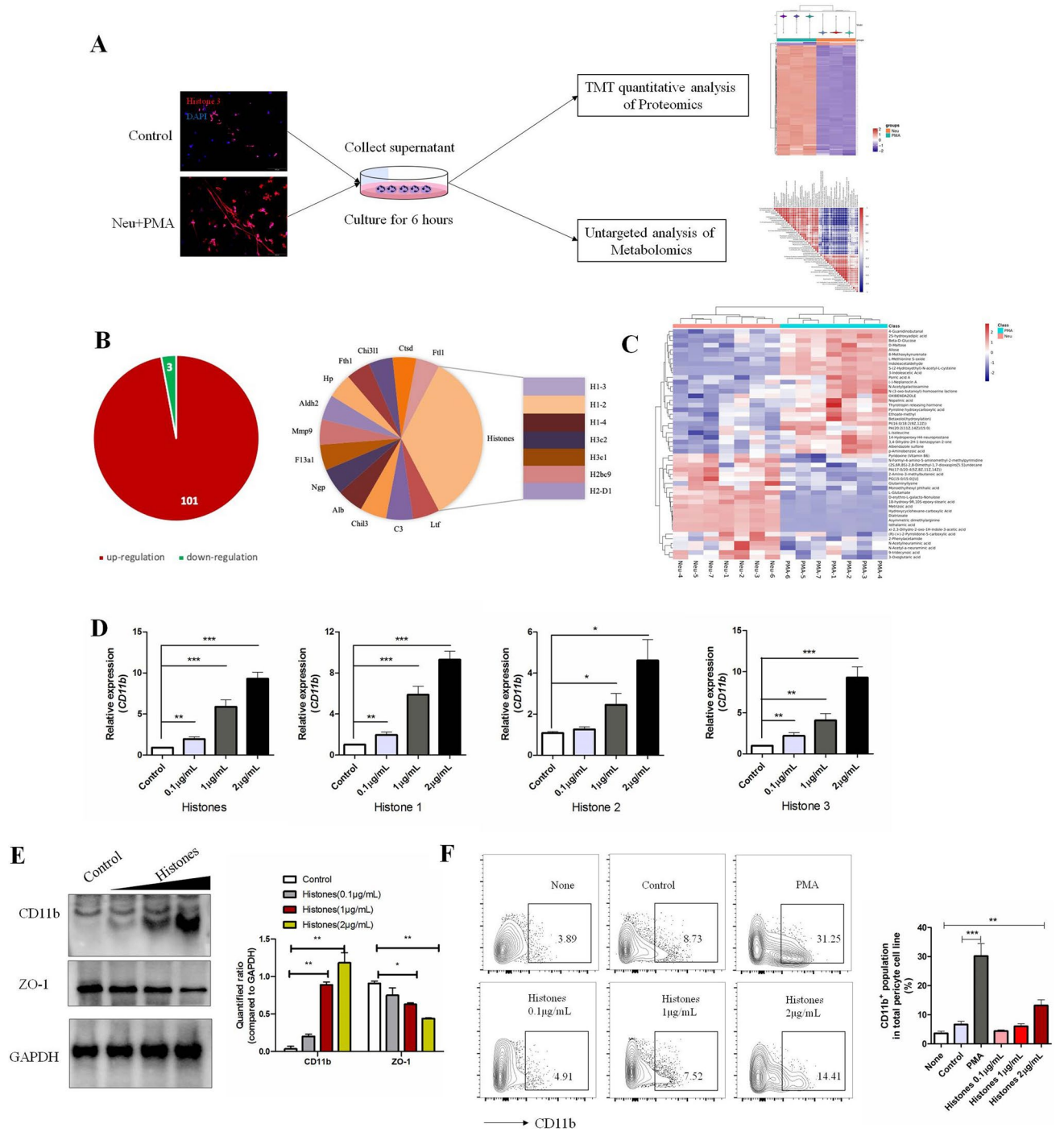

Fig. 5 Analysis of functional components from NET-formed medium affecting the pericyte phenotype. **A** Workflow for proteomics and metabolomics comparisons between NET-formed medium (PMA) and control medium (neutrophils without PMA stimulation) (proteomics, $n = 3$ per group; metabolomics, $n = 7$ per group). **B** Pie chart of differentially-expressed proteins and top 20 up-regulated proteins in NET-formed medium. Changes > 1.5-fold and $P < 0.05$ were considered significantly different. **C** Hierarchical clustering of differential metabolites in NET-formed medium. Differentially-expressed molecules repeatedly consistent in the same group with $P < 0.05$ were screened out and are highlighted in red (up-regulated) and blue (down-regulated). **D** RT-PCR analysis of relative CD11b mRNA expression in histone-treated MBVPs compared to controls. Cells were treated with recombinant histone peptides for 24 h. Histones are a mixture of histones 1, 2, and 3 at the a ratio of 1:1:1. **E** WB analysis of CD11b and ZO-1 in MBVPs incubated with histones for 48 h. Protein levels were quantified relative to GAPDH. **F** FACS analysis of the percentage of $CD11b^+$ MBVPs incubated under specific conditions for 48 h. Data are shown as the mean ± SEM of 3 individual experiments; $^*P < 0.05$, $^{**}P < 0.01$, $^{***}P < 0.001$, ANOVA.

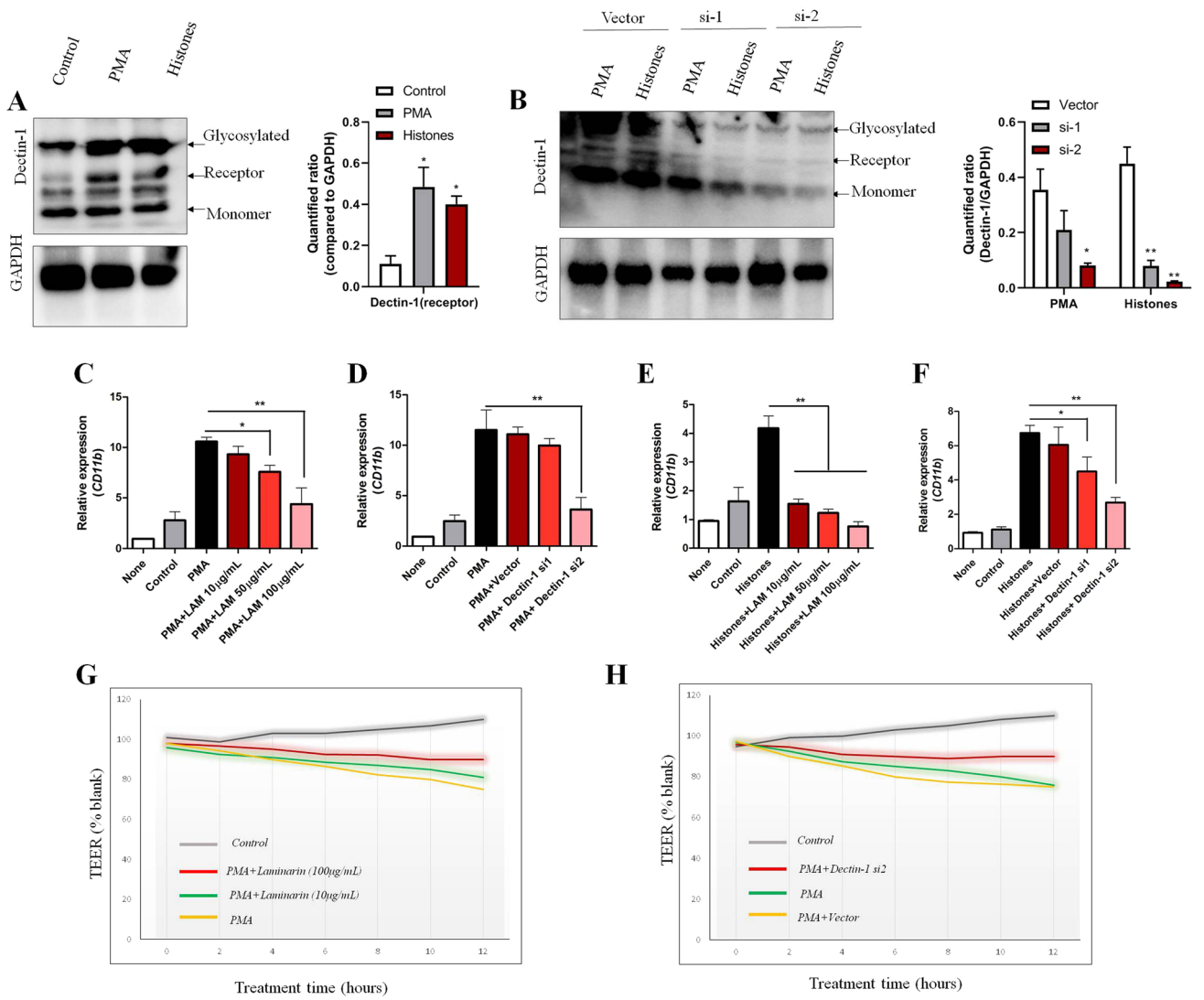

Fig. 6 Expression and function of Dectin-1 in brain pericytes. [Specific media: Control, medium from non-stimulated neutrophils; PMA, NET formation medium from neutrophils stimulated by PMA (100 ng/mL); Histones, mixed purified histone peptides (H1:H2:H3, 1:1:1) were dissolved at 2 μg/mL]. **A** WB analysis of Dectin-1expression on MBVPs incubated with specific media for 48 h (the specific medium was mixed with normal culture medium at a 1:3 ratio as described above). **B** WB analysis of Detin-1 expression on MBVPs stimulated with specific medium after transfecting blank vector or Dectin-1 siRNAs (si-1 and si-2). Dectin-1 protein levels were quantified relative to GAPDH. **C** Relative CD11b mRNA expression on MBVPs (compared to the none group) after NET-formed medium treatment combined with the indicated concentration of Dectin-1 antagonist LAM for 24 h. **D** Relative CD11b mRNA expression on MBVPs after NET-formed medium treatment combined with Dectin-1 siRNA transfection for 24 h (Vector, transfection solution without siRNAs). **E** Relative CD11b mRNA expression on MBVPs (compared to the none group) after Histones (2 μg/mL) treatment combined with indicated concentration of Dectin-1 for 24 h. **F** Relative CD11b mRNA expression on MBVPs after Histones (2 μg/mL) treatment combined with Dectin-1 siRNA transfection for 24 h (Vector, transfection solution without siRNAs). **G** Representative graph of continuous TEER values on MBVPs treated by NET-formed medium with/without the Dectin-1 antagonist Laminarin. **H** Representative graph of continuous TEER values on MBVPs treated with NET-formed medium with/without Dectin-1 siRNA transfection. TEER values for each group were compared to blank (MBVP under normal culture medium). Data are shown as the mean ± SEM of 5 individual experiments; *$P < 0.05$, **$P < 0.01$, one-way ANOVA.

with NET-formed medium or histones (Fig. 7A, B). In the presence of the Dectin-1 inhibitor LAM, Dectin-1 siRNAs, and the PKC inhibitor GFX, the phosphorylation levels of PKCζ/λ and c-Jun dropped dramatically (Fig. 7A, B), showing that Dectin-1 was essential for PKCζ/λ and c-Jun activation in response to NET-medium or histone stimulation. RT-PCR demonstrated that both the PKC inhibitor and the c-Jun inhibitor blunted the CD11b induction mediated

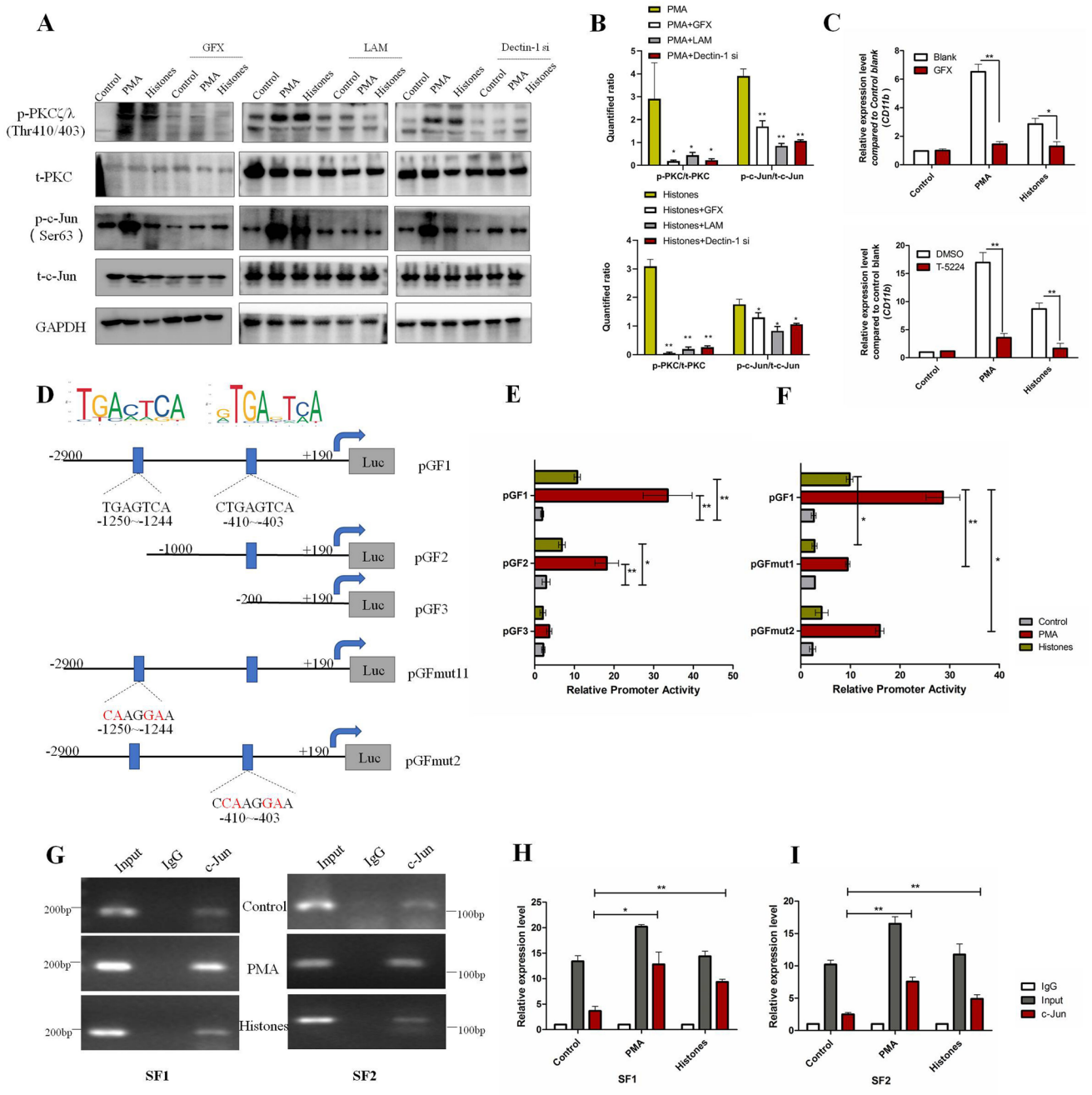

Fig. 7 PKC/c-Jun/CD11b pathways in histone/Dectin-1 recognition. **A** Representative WBs of total PKC (t-PKC), phosphorylated-PKCζ/λ (p-PKCζ/λ), total c-Jun (t-c-Jun), and phosphorylated-c-Jun in MBVPs treated with NET-formed medium (PMA) or Histones (2 μg/mL) with or without the PKC inhibitor GFX (5 μmol/L), Dectin-1 antagonist LAM (100 μg/mL), and siRNAs for 24 h. **B** Ratios of p-PKC/t-PKC and p-c-Jun/t-c-Jun in specific groups. Comparisons were made between PMA/Histones and combined treatment groups. **C** Relative expression of CD11b mRNA (compared to control blank group) on MBVPs treated with NET-formed medium (PMA) and Histones (2 μg/mL) for 24 h in the presence of GFX (5 μmol/L) or T-5224 (c-Jun inhibitor, 10 μmol/L). **D** Putative c-Jun binding sequence of the mouse CD11b promoter gene. **E** Luciferase activity of MBVPs co-transfected with indicated reporters under specific conditions. **F** Luciferase activity of MBVPs co-transfected with mutated reporters under specific conditions. All transfected cells were treated under the indicated conditions for 24 h and lysed for dual-luciferase measurements. **G** CHIP assays of the c-Jun binding sequence from the murine *CD11b* promoter gene. After treating MBVPs with the indicated conditions for 24 h, the total chromatin was collected and amplified as input (positive control). Antibody against c-Jun was used to pull down the binding segments, of which IgG was introduced as a negative control. Two pairs of specific primers that covered each binding site were used to amplify the SF1-containing segment (−1250 to −1244) and the SF2-containing segment (−410 to −403) within 30 cycles. **H, I** RT-PCR of CHIP products. qRT-PCR was performed with GAPDH as the internal reference gene and IgG in each group was the control. Data are shown as the mean ± SEM of 3 individual experiments; $^{**}P < 0.01$, $^{*}P < 0.05$, two-tailed unpaired Student's *t* test or ANOVA.

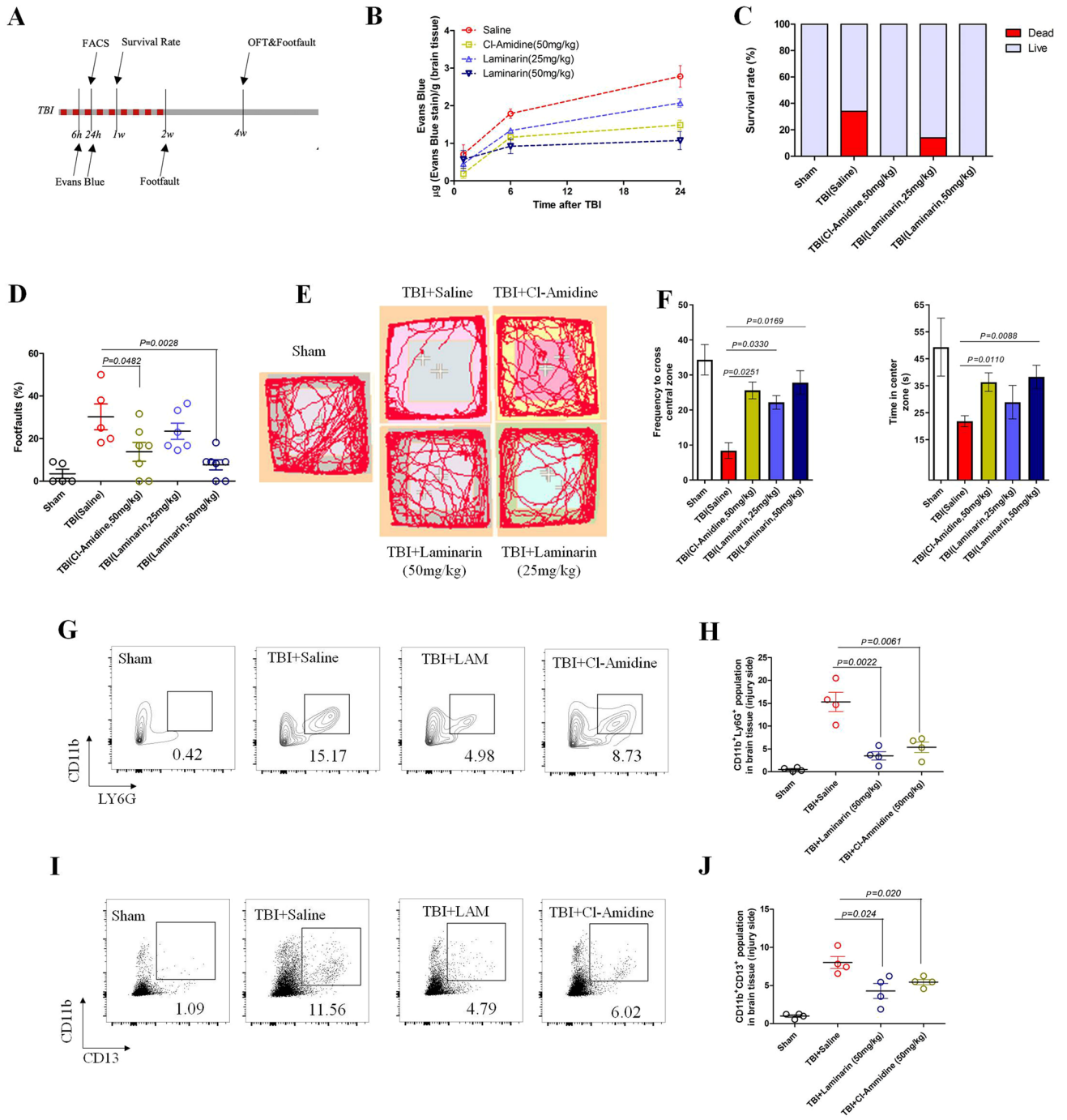

Fig. 8 Evaluation of BBB integrity, pericyte activation, neutrophil infiltration, and neurological recovery by targeting the NET–Dectin-1 axis post-TBI. **A** Schematic workflow of animal experiments. After constructing the moderate brain impact model, mice were immediately treated with the NET inhibitor Cl-Amidine (50 mg/kg) and the Dectin-1 antagonist Laminarin (25 and 50 mg/kg) by intraperitoneal injection every three days (5 injections). Two weeks later (red points), the treatments were terminated and mice were fed without any interference. **B** Quantification of Evans Blue in the left hemisphere (4 mice per group at the indicated time point). **C** Survival rate of each group in the first week after TBI impact with different treatments (n = 6 for Sham, n = 10 for TBI). **D** Footfault evaluation of TBI mice with administration of indicated drugs at 2 weeks post-injury ($n \geq 5$ per group). **E** Recordings of movement in OFT assessment at 4 weeks after moderate TBI impact with different treatments. **F** Frequency of crossing the central zone and time spent in the center zone of the OFT (as in **E**) ($n \geq 5$ per group). **G** FACS analysis of infiltrated neutrophils ($CD45^+CD11b^+LY6G^+$) from injured brain tissue at 24 h in TBI mice treated with the indicated drugs (n = 4 per group). **H** Quantification of neutrophils in brain tissue from each group (n = 4). **I** FACS analysis of $CD11b^+$ brain pericytes ($CD45^-CD11b^+CD13^+$) from brain tissue of TBI mice treated with the indicated drugs (n = 4 per group). **J** Quantification of $CD11b^+$ brain pericytes in brain tissue from each group (n = 4). Data are presented as the mean ± SEM, and analyzed by ANOVA. The animal numbers and P values of each group are shown in the figures and legends.

by NET-medium or histones (Fig. 7C). These data demonstrated that Dectin-1 contributed to the upregulation of CD11b expression in pericytes in response to NET-formed medium/histones through mediating PKCζ/λ-c-Jun signaling pathways.

c-Jun Directly Binds to the Promoter Sequence of CD11b to Enhance its Expression in Pericytes

c-Jun is an important transcription factor that modulates gene expression through binding to a promoter region. We next tested if c-Jun could activate *CD11b* transcription by binding to its promoter gene. After searching for possible c-Jun binding sites in the *CD11b* promoter gene region using NUBIScan, we screened out two possible sites with the "TGACTCA" motif (Figs 7D, S6). Subsequently, three luciferase reporters containing different promoter regions of the *CD11b* gene were constructed, as well as two mutant luciferase reporters that disrupted the binding motif. They were named pGF1 (−2900 to +190), pGF2 (−1000 to +190), pGF3 (−200 to +190), pGFmut1(−1250 to −1244), and pGFmut2 (−410 to −403) (Fig. 7D). The luciferase reporter assays showed that the activity of pGF1 and pGF2 was significantly increased in the presence of NET-formed medium or histones (Fig. 7E), revealing that these potential binding sites were capable of promoting *CD11b* gene expression. Of note, the ability of histones to raise *CD11b* promoter activity was relatively low compared to NET-formed medium (Fig. 7E), indicating that there were other potential components in NETs that induced CD11b expression apart from histones. Moreover, mutating these two sites separately both decreased the promoter activity (Fig. 7F), verifying that these sites were required for CD11b induction. ChIP assays further confirmed that c-Jun could bind to these two *CD11b* promoter regions (SF1: −1250 to −1244, SF2: −410 to −403, primers listed in Table S4) after stimulation with NET-formed medium or histones (Fig. 7G–I). Taken together, these results indicated that c-Jun activated CD11b expression by binding to two sites (−1250 to −1244 and −410 to −403) in the *CD11b* gene promoter region.

Inhibiting NET Formation and Blocking Dectin-1 both Improve Recovery of Brain Function after TBI

Previous studies and our results above confirm that NET formation and brain pericyte dysfunction contribute to acute TBI pathogenesis [18]. We further showed that histones of NETs facilitated CD11b induction of Dectin-1/PKC/c-Jun pathways in pericytes. It had been shown that blocking Dectin-1 is beneficial for ischemic injury in heart and brain [35, 36]. However, whether blocking NET formation and inhibiting Dectin-1 could decrease pericyte activation, restore BBB integrity, and improve the long-term outcome of TBI were undetermined. Thus, we explored the effects of Cl-Amidine (s NET inhibitor) and LAM (a Dectin-1 antagonist) at different time points after TBI (Fig. 8A). The mice were treated with or without Cl-Amidine (50 mg/kg) and LAM (25 and 50 mg/kg) intraperitoneally every three days post-TBI as in previous study [18, 35]. Administration of Cl-Amidine and LAM significantly reduced the BBB permeability and death rate in the acute phase compared with the saline group (Fig. 8B, C). These two drugs also improved motor and psychiatric functions in TBI mice after two/four weeks (Fig. 8D–F). FACS results also showed that Cl-Amidine and LAM dramatically decreased the amounts of infiltrated neutrophils (Fig. 8G, H) and $CD11b^+$ brain pericytes in injured brains within 24 h after TBI (Fig. 8I, J), resulting in neurobehavioral improvement. These data provided evidence that targeting NET formation and Dectin-1 effectively ameliorates BBB disruption and neutrophil infiltration, facilitating neurological recovery after TBI.

Discussion

In this study, we report for the first time that histones of NETs induce CD11b expression in brain pericytes. $CD11b^+$ pericytes express pro-inflammatory molecules more strongly than $CD11b^-$ pericytes, leading to BBB disruption and increased leukocyte infiltration. Mechanistically, Dectin-1 in pericytes is responsible for recognizing histones to induce CD11b expression in a PKC-c-Jun-dependent manner. These data indicate that NET formation is associated with BBB disruption by inducing CD11b expression in brain pericytes. Neutrophils→NETs→pericytes and histones→Dectin-1→CD11b" are possible cellular and molecular mechanisms for building connections between BBB disruption and neutrophil infiltration.

Pericytes are generally treated as indispensable participants during the regulation of angiogenesis and microcirculation [7, 37]. Under pathological conditions, activated pericytes mediate neuroinflammation in diverse ways, including leukocyte recruitment and BBB disruption [9], pericyte-endothelium communications [38], the formation of fibrotic scars [39], and endocytosis [40]. Hence, future studies of the functions and phenotypes of $CD11b^+$ brain pericytes in the pathogenesis of TBI are desperately needed.

In brain diseases, it has been shown that NETs are associated with cerebral edema, hypoperfusion, BBB damage, neurotoxicity, and amyloid β plaque deposition [15, 18]. Previous studies have shown that circulating histones from necrotic or dead cells are closely associated with several brain diseases [41, 42]. Our study builds the connections between NET histones and CD11b induction in brain pericytes, providing possible histone-related molecular

mechanism in neuroinflammation. Of note, there are two forms of NET structure: suicidal NETosis and vital NETosis [43]. In suicidal NETosis, dead neutrophils spill out segmented chromatins and intracellular granules, while vital NETosis generally forms when neutrophils remain alive and release only parts of their nuclear or mitochondrial DNA without antibacterial proteins and granules [44]. In the present study, we mainly focused on the effects mediated by extracellular spillage when soluble NETs (suicidal NETosis) are formed. The differences of extracellular components and effects between vital and suicidal NETosis deserve further exploration.

Previous studies and our data (Fig. S5B, C) showed that histones contain some amino-acid residues such as lysine, arginine, and histidine, that are critical for recognition by Clec2d [31]. We speculated that Dectin-1 might bind to histones dependent on these residues since Dectin-1 and Clec2d share similar binding domains (Fig. S5B); this needs to be verified in the future. Based on the latest study, Dectin-1 was strongly enhanced in brain tissue following ischemic injury or TBI, causing overwhelming activation of microglia [35, 45]. This provides a hint that Dectin-1 might affect neuroinflammation in multiple ways. Li *et al.* also found that Dectin-1 facilitates CD11b activation by forming the Vav-PLCγ complex during fungal clearance [46], raising the possibility that Dectin-1 modulates the functions of CD11b by changing either the expression level or activation status.

In conclusion, our data support the hypothesis that NET-associated histones promote the formation of $CD11b^+$ brain pericytes in TBI. Recognition of the histones on pericytes by Dectin-1 contributes to CD11b induction in a PKC-c-Jun-dependent manner. Targeting NET formation and Dectin-1 are efficient means of restoring BBB integrity and decreasing neutrophil infiltration to improve the neurological outcomes of TBI.

Acknowledgements This work was supported by the National Natural Science Foundation of China (32000670 and 82071779) and Chongqing Research Program of Basic Research and Frontier Technology (cstc2017jcyjAX0338).

Conflict of interest The authors all declare that they have no competing interests.

References

1. Luo JN, Wu X, Liu HX, Cui WX, Guo W, Guo K. Antagonism of protease-activated receptor 4 protects against traumatic brain injury by suppressing neuroinflammation via inhibition of Tab2/NF-κB signaling. Neurosci Bull 2021, 37: 242–254.
2. Jing Y, Yang DX, Wang W, Yuan F, Chen H, Ding J, *et al*. Aloin protects against blood-brain barrier damage after traumatic brain injury in mice. Neurosci Bull 2020, 36: 625–638.
3. Williams OH, Tallantyre EC, Robertson NP. Traumatic brain injury: Pathophysiology, clinical outcome and treatment. J Neurol 2015, 262: 1394–1396.
4. Kolaczkowska E, Kubes P. Neutrophil recruitment and function in health and inflammation. Nat Rev Immunol 2013, 13: 159–175.
5. Shi YJ, Zhang LL, Pu HJ, Mao LL, Hu XM, Jiang XY, *et al*. Rapid endothelial cytoskeletal reorganization enables early blood-brain barrier disruption and long-term ischaemic reperfusion brain injury. Nat Commun 2016, 7: 10523.
6. Liebner S, Dijkhuizen RM, Reiss Y, Plate KH, Agalliu D, Constantin G. Functional morphology of the blood-brain barrier in health and disease. Acta Neuropathol 2018, 135: 311–336.
7. Sweeney MD, Ayyadurai S, Zlokovic BV. Pericytes of the neurovascular unit: Key functions and signaling pathways. Nat Neurosci 2016, 19: 771–783.
8. Smyth LCD, Rustenhoven J, Park TIH, Schweder P, Jansson D, Heppner PA, *et al*. Unique and shared inflammatory profiles of human brain endothelia and pericytes. J Neuroinflammation 2018, 15: 138.
9. Rustenhoven J, Jansson D, Smyth LC, Dragunow M. Brain pericytes as mediators of neuroinflammation. Trends Pharmacol Sci 2017, 38: 291–304.
10. Proebstl D, Voisin MB, Woodfin A, Whiteford J, D'Acquisto F, Jones GE, *et al*. Pericytes support neutrophil subendothelial cell crawling and breaching of venular walls *in vivo*. J Exp Med 2012, 209: 1219–1234.
11. Hutter-Schmid B, Humpel C. Primary mouse brain pericytes isolated from transgenic Alzheimer mice spontaneously differentiate into a CD11b + microglial-like cell type *in vitro*. Exp Gerontol 2018, 112: 30–37.
12. Özen I, Deierborg T, Miharada K, Padel T, Englund E, Genové G, *et al*. Brain pericytes acquire a microglial phenotype after stroke. Acta Neuropathol 2014, 128: 381–396.
13. Yipp BG, Kubes P. NETosis: how vital is it? Blood 2013, 122: 2784–2794.
14. Tan CY, Aziz M, Wang P. The vitals of NETs. J Leukoc Biol 2021, 110: 797–808.
15. Manda-Handzlik A, Demkow U. The brain entangled: The contribution of neutrophil extracellular traps to the diseases of the central nervous system. Cells 2019, 8: 1477.
16. Kang LJ, Yu HL, Yang X, Zhu YB, Bai XF, Wang RR, *et al*. Neutrophil extracellular traps released by neutrophils impair revascularization and vascular remodeling after stroke. Nat Commun 2020, 11: 2488.
17. Zeng HH, Fu XJ, Cai J, Sun CJ, Yu MY, Peng YC, *et al*. Neutrophil extracellular traps may be a potential target for treating early brain injury in subarachnoid hemorrhage. Transl Stroke Res 2022, 13: 112–131.
18. Vaibhav K, Braun M, Alverson K, Khodadadi H, Kutiyanawalla A, Ward A, *et al*. Neutrophil extracellular traps exacerbate neurological deficits after traumatic brain injury. Sci Adv 2020, 6: eaax8847.
19. Yipp BG, Petri B, Salina D, Jenne CN, Scott BNV, Zbytnuik LD, *et al*. Infection-induced NETosis is a dynamic process involving neutrophil multitasking *in vivo*. Nat Med 2012, 18: 1386–1393.
20. Yang T, Liu YW, Zhao L, Wang H, Yang N, Dai SS, *et al*. Metabotropic glutamate receptor 5 deficiency inhibits neutrophil infiltration after traumatic brain injury in mice. Sci Rep 2017, 7: 9998.
21. Liu YW, Yang T, Zhao L, Ni ZH, Yang N, He FT, *et al*. Activation of Adenosine 2A receptor inhibits neutrophil apoptosis in an autophagy-dependent manner in mice with systemic inflammatory response syndrome. Sci Rep 2016, 6: 33614.
22. Crouch EE, Doetsch F. FACS isolation of endothelial cells and pericytes from mouse brain microregions. Nat Protoc 2018, 13: 738–751.

23. Rathmann D, Rijntjes E, Lietzow J, Köhrle J. Quantitative analysis of thyroid hormone metabolites in cell culture samples using LC-MS/MS. Eur Thyroid J 2015, 4: 51–58.
24. Wang ZK, Liu FJ, Ye SL, Jiang P, Yu XC, Xu J, *et al*. Plasma proteome profiling of high-altitude polycythemia using TMT-based quantitative proteomics approach. J Proteomics 2019, 194: 60–69.
25. Devraj G, Guérit S, Seele J, Spitzer D, Macas J, Khel MI, *et al*. HIF-1α is involved in blood-brain barrier dysfunction and paracellular migration of bacteria in pneumococcal meningitis. Acta Neuropathol 2020, 140: 183–208.
26. Zhao L, Liu YW, Yang T, Gan L, Yang N, Dai SS, *et al*. The mutual regulation between miR-214 and A2AR signaling plays an important role in inflammatory response. Cell Signal 2015, 27: 2026–2034.
27. Liu YW, Zhao L, Zhou M, Wang H, Yang N, Dai SS. Transplantation with mGluR5 deficiency bone marrow displays antidepressant-like effect in C57BL/6J mice. Brain Behav Immun 2019, 79: 114–124.
28. Bajwa NM, Lee JB, Halavi S, Hartman RE, Obenaus A. Repeated isoflurane in adult male mice leads to acute and persistent motor decrements with long-term modifications in corpus callosum microstructural integrity. J Neurosci Res 2019, 97: 332–345.
29. Mao XB, Qi S, Yu B, He J, Yu J, Chen DW. Zn(2+) and L-isoleucine induce the expressions of porcine β-defensins in IPEC-J2 cells. Mol Biol Rep 2013, 40: 1547–1552.
30. Huang HC, Lin H, Huang MC. Lactoferrin promotes hair growth in mice and increases dermal papilla cell proliferation through Erk/Akt and Wnt signaling pathways. Arch Dermatol Res 2019, 311: 411–420.
31. Lai JJ, Cruz FM, Rock KL. Immune sensing of cell death through recognition of histone sequences by C-type lectin-receptor-2d causes inflammation and tissue injury. Immunity 2020, 52: 123-135.e6.
32. Drouin M, Saenz J, Chiffoleau E. C-type lectin-like receptors: Head or tail in cell death immunity. Front Immunol 2020, 11: 251.
33. Patin EC, Orr SJ, Schaible UE. Macrophage inducible C-type lectin as a multifunctional player in immunity. Front Immunol 2017, 8: 861.
34. Nikolakopoulou C, Willment JA, Brown GD. C-type lectin receptors in antifungal immunity. Adv Exp Med Biol 2020, 1204: 1–30.
35. Ye XC, Hao Q, Ma WJ, Zhao QC, Wang WW, Yin HH, *et al*. Dectin-1/Syk signaling triggers neuroinflammation after ischemic stroke in mice. J Neuroinflammation 2020, 17: 17.
36. Fan Q, Tao R, Zhang H, Xie HY, Lu L, Wang T, *et al*. Dectin-1 contributes to myocardial ischemia/reperfusion injury by regulating macrophage polarization and neutrophil infiltration. Circulation 2019, 139: 663–678.
37. Liu Q, Lin WJ, Tang YM. New insights into the dysfunctions of pericytes and neurovascular units in neurodegenerative diseases. Neurosci Bull 2020, 36: 1570–1572.
38. Bhowmick S, D'Mello V, Caruso D, Wallerstein A, Abdul-Muneer PM. Impairment of pericyte-endothelium crosstalk leads to blood-brain barrier dysfunction following traumatic brain injury. Exp Neurol 2019, 317: 260–270.
39. Hesp ZC, Yoseph RY, Suzuki R, Jukkola P, Wilson C, Nishiyama A, *et al*. Proliferating NG2-cell-dependent angiogenesis and scar formation alter axon growth and functional recovery after spinal cord injury in mice. J Neurosci 2018, 38: 1366–1382.
40. Ojo J, Eisenbaum M, Shackleton B, Lynch C, Joshi U, Saltiel N, *et al*. Mural cell dysfunction leads to altered cerebrovascular tau uptake following repetitive head trauma. Neurobiol Dis 2021, 150: 105237.
41. Shah M, Yellon DM, Davidson SM. The role of extracellular DNA and histones in ischaemia-reperfusion injury of the myocardium. Cardiovasc Drugs Ther 2020, 34: 123–131.
42. Szatmary P, Huang W, Criddle D, Tepikin A, Sutton R. Biology, role and therapeutic potential of circulating histones in acute inflammatory disorders. J Cell Mol Med 2018, 22: 4617–4629.
43. Rada B. Neutrophil extracellular traps. Methods Mol Biol 1982, 2019: 517–528.
44. Yousefi S, Stojkov D, Germic N, Simon D, Wang XL, Benarafa C, *et al*. Untangling "netosis" from NETs. Eur J Immunol 2019, 49: 221–227.
45. Fu XJ, Zeng HH, Zhao JK, Zhou GY, Zhou H, Zhuang JF, *et al*. Inhibition of dectin-1 ameliorates neuroinflammation by regulating microglia/macrophage phenotype after intracerebral hemorrhage in mice. Transl Stroke Res 2021, 12: 1018–1034.
46. Li X, Utomo A, Cullere X, Choi MM, Milner DA Jr, Venkatesh D, *et al*. The β-glucan receptor Dectin-1 activates the integrin Mac-1 in neutrophils via Vav protein signaling to promote *Candida albicans* clearance. Cell Host Microbe 2011, 10: 603–615.